

Differential Cross Sections for Higgs Production

V. Ravindran

Harish-Chandra Research Institute,
Chhatnag Road, Jhansi,
Allahabad, 211019, India.

J. Smith

C.N. Yang Institute for Theoretical Physics,
State University of New York at Stony Brook, New York 11794-3840, USA.

W. L. van Neerven

Instituut-Lorentz
University of Leiden,
P.O. Box 9506, 2300 RA Leiden,
The Netherlands.

Abstract

We review recent theoretical progress in evaluating higher order QCD corrections to Higgs boson differential distributions at hadron-hadron colliders.

1 Introduction

The origin of the spontaneous symmetry breaking mechanism (ssbm) in particle physics is still unknown. In the Standard Model (SM) [1] a vacuum expectation value (vev) $v = 246 \text{ GeV}$ is given to components of a complex scalar doublet. Three of these fields generate mass terms for the W and Z bosons. The remaining scalar is called the Higgs [2] and has not been observed. The present lower limit for m_H from the LEP experiments [3] is $114 \text{ GeV}/c^2$. In the SM the interaction vertices with scalar fields are expressed in terms of v and m_H . Extensions of the standard model to incorporate supersymmetry contain several Higgs particles, both scalar and pseudoscalar [4]. In the minimal supersymmetric extension of the Standard Model (MSSM), there are two Higgs doublets, so it is called the Two-Higgs-Doublet Model (2HDM). After implementing the ssbm there are five Higgs bosons usually denoted by h, H , (CP even), A (CP odd) and H^\pm . At tree level their couplings and masses depend on two parameters, m_A and the ratio of two vevs, parametrized by $\tan\beta = v_2/v_1$. Since no Higgs particle has been found the region $m_A < 92 \text{ GeV}/c^2$ and $0.5 < \tan\beta < 2.4$ is experimentally excluded [5]. For recent reviews on the theoretical status of total Higgs boson cross sections see [6]. Let us denote the neutral bosons h, H, A collectively by B . It is possible that a B will be detected at the Fermilab Tevatron $p\bar{p}$ collider ($\sqrt{s} = 2 \text{ TeV}$). If not it should hopefully be found at the Large Hadron Collider (LHC), a $p\bar{p}$ machine under construction at CERN ($\sqrt{s} = 14 \text{ TeV}$). If no B is found then the ssbm must be realized in a different way, possibly via dynamical interactions between the gauge bosons. In parallel with the ongoing experimental and higher order quantum chromodynamic (QCD) corrections to B production differential distributions are needed. The leading order (LO)

partonic reactions were calculated quite a long time ago and the next-to-leading order (NLO) corrections to these distributions only recently. Note that the detection of the B via its decay products depends on m_B . The present mass limits allow the decays $B \rightarrow \mu\mu$, $B \rightarrow b\bar{b}$ and $B \rightarrow W^+W^-; ZZ$ where W and Z are virtual vector bosons, which are detected as leptons and/or hadrons (jets). As m_B increases other decay channels (for example $B \rightarrow W^+W^-; ZZ$, $B \rightarrow t\bar{t}$), open up requiring different experimental triggers. Higher order QCD corrections to these decay rates have also been calculated but will not be discussed here.

2 Higgs differential distributions

For inclusive B -production one calculates the differential cross section in the B transverse momentum (p_T) and its rapidity (y), which are functions of m_B , the partonic momentum fractions x_1, x_2 in the hadron beams, and the partonic energy $\sqrt{s} = \sqrt{x_1 x_2 S}$. All other final state particles are integrated over. In contrast exclusive B -production retains the information on these other particles. In the SM the H couples to the gluons via quark loops with the $q\bar{q}H$ vertex proportional to m_q , so the t -quark loop is the most important. In the 2HDM the ggA amplitude with quark loops depends on both the masses of the quarks and $\tan\beta$. In LO the $g + g \rightarrow H$ cross section (order α_s^2) containing the top-quark triangle graph, was computed in [7]. However here $p_T = 0$, so we need a two-to-two body partonic process to produce a Higgs with a finite p_T . Note that these are NLO processes with respect to the total B production cross section and of order α_s^3 . At small x the gluon density $g(x; Q^2) > q_i(x; Q^2) > \bar{q}_i(x; Q^2)$, (q_i stand for $u; d; s; c; b; t$ quarks) so we expect that, in order of importance, the dominant production channels are

$$\begin{aligned} g + g &\rightarrow g + B; \\ g + q_i(\bar{q}_i) &\rightarrow q_i(\bar{q}_i) + B; \\ q_i + \bar{q}_i &\rightarrow g + B; \end{aligned} \tag{2.1}$$

These are the LO order Born reactions for Higgs p_T and y distributions. The corresponding Feynman diagrams contain heavy quark box graphs. The B differential distributions for the reactions in Eq. (2.1) were computed for $B=H$ in [8] and for $B=A$ in [9]. The total cross section, which also contains the virtual QCD corrections to the ggB top-quark triangle, was calculated in [10], [11] and [12]. The expressions in [12] for the two-loop graphs with finite m_t and m_B are very complicated. Furthermore also the two-to-three body reactions (e.g. $g + g \rightarrow g + g + B$ involving pentagon loops) have been computed in [13] using helicity methods. From these results it is clear that it will be very difficult to obtain the NLO (order α_s^4) corrections to the B differential distributions as functions of both m_t and m_B .

Fortunately one can simplify the calculations if one takes the limit $m_t \rightarrow \infty$. In this case the Feynman graphs are obtained from an effective Lagrangian describing the direct Bgg coupling. An analysis in [14] in NLO reveals that the error introduced by taking the $m_t \rightarrow \infty$ limit is less than about 5% provided $m_B \geq 2m_t$. The two-to-three body processes were computed with the effective Lagrangian approach for the B in [15] and [16] respectively using helicity methods. The one-loop corrections to the two-to-two body reactions above were computed for the H in [17] and the A in [9]. These NLO matrix elements (order α_s^4) were used to compute the p_T and y distributions of the H in [18], [19], [20], [21] and the A in [22]. For ways to differentiate between production of H and A see [23] and references therein.

In the large m_t limit the Feynman rules (see e.g. [15]) for scalar H production can be derived from the following effective Lagrangian density

$$L_{\text{eff}}^H = G_H H(x) O(x) \quad \text{with} \quad O(x) = \frac{1}{4} G^a(x) G^a(x); \quad (2.2)$$

whereas pseudoscalar A production is obtained from

$$L_{\text{eff}}^A = A(x) G_A O_1(x) + \tilde{G}_A O_2(x); \quad \text{with} \\ O_1(x) = \frac{1}{8} G_a(x) G_a(x); \quad O_2(x) = \frac{1}{2} \partial_{\mu} \sum_{i=1}^{n_f} q_i(x) \gamma_5 q_i(x); \quad (2.3)$$

where $H(x)$ and $A(x)$ represent the scalar and pseudoscalar fields respectively and n_f denotes the number of light flavours. Furthermore the gluon field strength tensor is given by $G_a(x)$ (a is the colour index) and the quark field is denoted by $q_i(x)$. The factors in the definitions of O, O_1 and O_2 are chosen in such a way that the vertices are normalised to the effective coupling constants G_H, G_A and \tilde{G}_A . The latter are determined by the triangular loop graphs, which describe the decay processes $B \rightarrow g + g$ with $B = H, A$, including all QCD corrections and taken in the limit $m_t \rightarrow \infty$, namely

$$G_B = 2^{5=4} a_s(\frac{2}{r}) G_F^{1=2} F_B(\beta) C_B a_s(\frac{2}{r}); \frac{2}{m_t^2}; \\ \tilde{G}_A = a_s(\frac{2}{r}) C_F \left[\frac{3}{2} \ln \frac{2}{m_t^2} + \right] G_A; \quad (2.4)$$

where $a_s(\frac{2}{r})$ is defined by

$$a_s(\frac{2}{r}) = \frac{s(\frac{2}{r})}{4}; \quad (2.5)$$

with $s(\frac{2}{r})$ the running coupling constant and r the renormalization scale. Further G_F represents the Fermi constant and the functions F_B are given by

$$F_H(\beta) = 1 + (1 - \beta^2) f(\beta); \quad F_A(\beta) = f(\beta) \cot \beta; \quad \beta = \frac{4m_t^2}{m_B^2}; \\ f(\beta) = \arcsin^2 \frac{1}{\beta}; \quad \text{for} \quad \beta \geq 1; \\ f(\beta) = \frac{1}{4} \ln \frac{1 + \frac{\beta}{1 + \beta}}{1 - \frac{\beta}{1 + \beta}} + \frac{\pi^2}{4} \quad \text{for} \quad \beta < 1; \quad (2.6)$$

where β denotes the mixing angle in the 2HDM. In the large m_t limit we have

$$\lim_{\beta \rightarrow 1} F_H(\beta) = \frac{2}{3}; \quad \lim_{\beta \rightarrow 1} F_A(\beta) = \frac{1}{3} \cot \beta; \quad (2.7)$$

The coefficient functions C_B originate from the corrections to the top-quark triangle graph provided one takes the limit $m_t \rightarrow \infty$. The coefficient functions were computed up to order $\frac{2}{s}$ in

[14], [24] for the H and in [25] for the A . The answer depends upon $a_s^{(5)}$, the running coupling in the $\overline{\text{MS}}$ scheme, and we only need the first order terms

$$\begin{aligned} C_H(a_s(\frac{s}{m_t^2}); \frac{s}{m_t^2}) &= 1 + 11a_s^{(5)} + \dots \\ C_A(a_s(\frac{s}{m_t^2}); \frac{s}{m_t^2}) &= 1: \end{aligned} \quad (2.8)$$

The last result holds to all orders because of the Adler-Bardeen theorem [26].

3 Numerical results at moderate p_T

The hadronic cross section $d\sigma_{H_1(P_1)+H_2(P_2) \rightarrow B(P_5)+X}$ is obtained from the partonic cross sections $d\sigma_{ab}$ for the reactions in Eq. (2.1) and their NLO corrections [for example $g(p_1) + g(p_2) \rightarrow g(p_3) + g(p_4) + B(p_5)$] using

$$\begin{aligned} S^2 \frac{d^2 \sigma_{H_1 H_2}}{d T d U}(S; T; U; m_B^2) &= \sum_{a,b=q\bar{q}} \int_{x_{1\min}}^{x_{1\max}} \frac{dx_1}{x_1} \int_{x_{2\min}}^{x_{2\max}} \frac{dx_2}{x_2} f_a^{H_1}(x_1; \mu^2) \\ &\quad f_b^{H_2}(x_2; \mu^2) s^2 \frac{d^2 \sigma_{ab}}{d t d u}(s; t; u; m_B^2; \mu^2): \end{aligned} \quad (3.9)$$

Here $f_a^H(x; \mu^2)$ is the parton density for parton a in hadron H at factorization/renormalization scale μ and the hadronic kinematical variables are defined by

$$S = (P_1 + P_2)^2; \quad T = (P_1 + P_5)^2; \quad U = (P_2 + P_5)^2: \quad (3.10)$$

The latter two invariants can be expressed in terms of the p_T and y variables by

$$\begin{aligned} T &= m_B^2 \frac{p_{-q}}{S} \frac{1}{p_T^2 + m_B^2} \cosh y + \frac{p_{-q}}{S} \frac{1}{p_T^2 + m_B^2} \sinh y; \\ U &= m_B^2 \frac{p_{-q}}{S} \frac{1}{p_T^2 + m_B^2} \cosh y - \frac{p_{-q}}{S} \frac{1}{p_T^2 + m_B^2} \sinh y: \end{aligned} \quad (3.11)$$

In the case parton p_1 emerges from hadron $H_1(P_1)$ and parton p_2 emerges from hadron $H_2(P_2)$ we can establish the following relations

$$\begin{aligned} p_1 &= x_1 P_1; \quad p_2 = x_2 P_2; \\ s &= x_1 x_2 S; \quad t = x_1 (T - m_B^2) + m_B^2; \quad u = x_2 (U - m_B^2) + m_B^2; \\ x_{1\min} &= \frac{U}{S + T - m_B^2}; \quad x_{2\min} = \frac{x_1 (T - m_B^2) - m_B^2}{x_1 S + U - m_B^2}: \end{aligned} \quad (3.12)$$

Since the differential cross section contains terms $\ln^i(m_B/p_T)$, ($i = 1; 2; 3$) which are not integrable at $p_T = 0$, we cannot integrate over p_T down to $p_T = 0$ to find the y -distribution. However we can integrate over y to find the p_T -distribution, valid over a range in p_T where there are no large logarithms, (say $p_T > 30 \text{ GeV} = c$),

$$\frac{d \sigma_{H_1 H_2}}{d p_T}(S; p_T^2; m_B^2) = \int_{y_{\min}}^{y_{\max}} dy \frac{d^2 \sigma_{H_1 H_2}}{d p_T dy}(S; p_T^2; y; m_B^2); \quad (3.13)$$

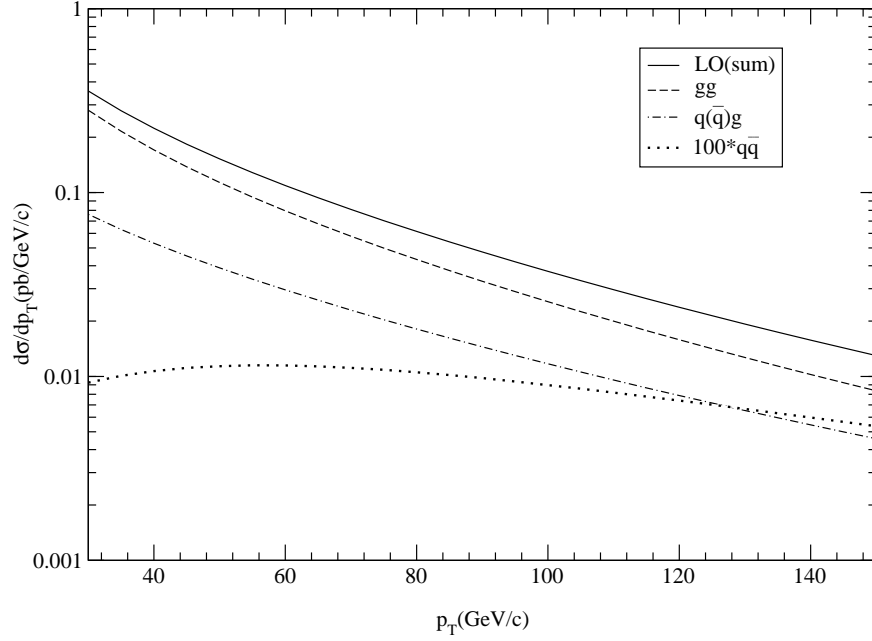


Figure 1: The differential cross section $d\sigma/dp_T$ integrated over the whole rapidity range (see Eq. (3.13)) with $m_H = 120 \text{ GeV} = c^2$ and $s^2 = m_H^2 + p_T^2$. The LO plots are presented for the subprocesses gg (long-dashed line), $q(q)g$ (dot-dashed line) and $100 \cdot qq$ (dotted line) using the parton density set MRST 98 (lo05a.dat).

with a fixed y_{max} . The calculation of the NLO B differential distributions requires the virtual corrections to the reactions in Eq. (2.1) and the NLO two-to-three body reactions (order s^4). Hence one needs a regularization scheme, and renormalization and mass factorization (which introduces the scales μ_r and μ_f respectively). The presence of the s matrix in the pseudoscalar contributions makes everything even more complicated and we refer to [22] for details. In [18] helicity amplitudes were used and the fully exclusive two-to-three body reactions were calculated numerically. Very few formulae were presented. In [19] the cancellations of the UV and IR singularities were done algebraically leading to the H inclusive distributions. Many analytical results were given but the two-to-three body matrix elements were too long to publish. In [20], [21] helicity amplitudes were used for the H inclusive calculation and complete analytical results were provided. The numerical results from these three papers have been compared against each other and they agree.

We put $n_f = 5$ in $a_s(\mu_r^2)$, α_{ab} and $f_a^H(x; s^2)$ in Eq.(3.9). For simplicity $\mu_r = \mu_f = \mu$ and we take $s^2 = m_H^2 + p_T^2$ for our plots. Further we have used the parton density sets MRST 98 [27], MRST 99 [28], GRV 98 [29], CTEQ 4 [30] and CTEQ 5 [31].

We want to emphasize that the magnitudes of the cross sections are extremely sensitive to the choice of the renormalization scale because the effective coupling constants in Eq.(2.4) are proportional to $\alpha_s(\mu_r)$, which implies that $d^{\text{LO}} \propto s^3$ and $d^{\text{NLO}} \propto s^4$. However the slopes of the differential distributions are less sensitive to the scale choice if they are only plotted over a limited range. For the computation of the ggB effective coupling constants in Eq. (2.4) we take $m_t = 173.4 \text{ GeV} = c^2$ and $G_F = 1.16639 \text{ GeV}^{-2} = 4541.68 \text{ pb}$. Here we will only give results for H production at the LHC. Lack of space limits us to showing only p_T -distributions. The LO and NLO p_T differential cross sections in Eq. (3.13) with $m_H = 120 \text{ GeV} = c^2$ are shown in Figs. 1 and 2 respectively. The MRST 98 parton densities [27] were used for these plots. We note that

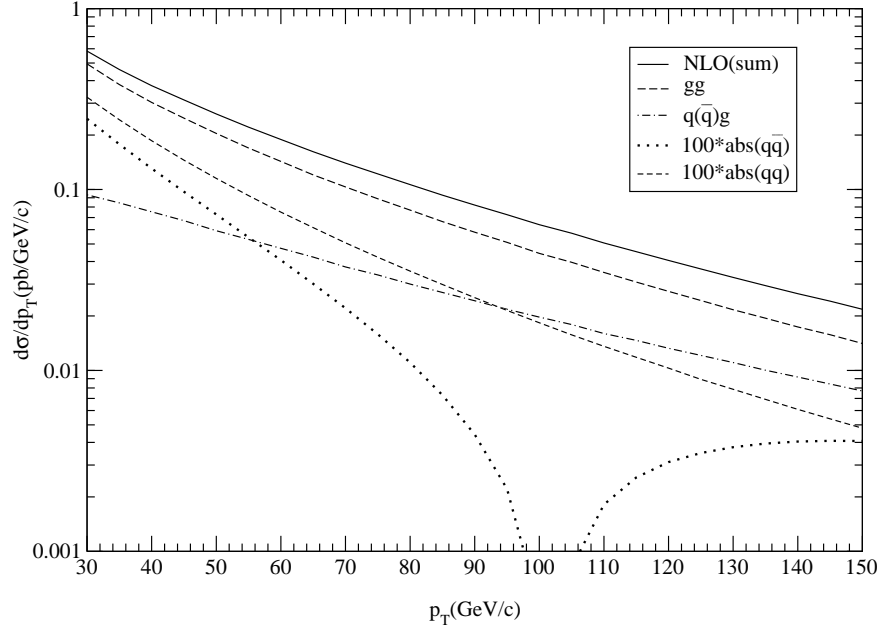


Figure 2: Same as Fig. 1 in NLO except for $100 \text{ abs}(qq)$ (dotted line) and the additional subprocess $100 \text{ abs}(qq)$ (short-dashed line) using the parton density set MRST 98 (ff08a.dat).

the NLO results from the $q(q)g$ and qq channels are negative at small p_T so we have plotted their absolute values multiplied by 100. Clearly the gg reaction dominates. The $q(q)g$ reaction is lower by a factor of about five.

Regarding the corresponding distributions for A -production they have the same shape dependence in LO and differ slightly in NLO. Therefore the only difference is in the overall couplings in Eq. (2.4). In particular if $\tan \beta = 1$ then $d_A = d_H = 9/4$ for all values of m_H and m_A in LO. There are small differences from $9/4$ in NLO. Plots are presented in [22].

We now show the scale dependence of the distributions. We have chosen the scale factors $\mu = 2\mu_0$, $\mu = \mu_0$ and $\mu = \mu_0/2$ with $\mu_0^2 = m_H^2 + p_T^2$ and plot in Fig. 3 the quantity

$$N(p_T; \mu) = \frac{d(p_T; \mu)/dp_T}{d(p_T; \mu_0)/dp_T} \quad (3.14)$$

in the range $0.1 < \mu/\mu_0 < 10$ at fixed values of $p_T = 30, 70$ and $100 \text{ GeV}/c$. The upper set of curves at small μ/μ_0 are for LO and the lower set are for NLO. Notice that the NLO plots at 70 and 100 are extremely close to each other and it is hard to distinguish between them. One sees that the slopes of the LO curves are larger than the slopes of the NLO curves. This is an indication that there is a small improvement in stability in NLO, which was expected. However there is no sign of a flattening or an optimum in either of these curves which implies that one will have to calculate the differential cross sections in NNLO to find a better stability under scale variations.

Next we show the mass dependence of the NLO result in Fig. 4 using the MRST 99 parton densities. The differential distribution drops by a factor of two as m_H increases from 120 to 180 GeV/c^2 .

There are two other uncertainties which affect the predictive power of the theoretical cross sections. The first one concerns the rate of convergence of the perturbation series which is

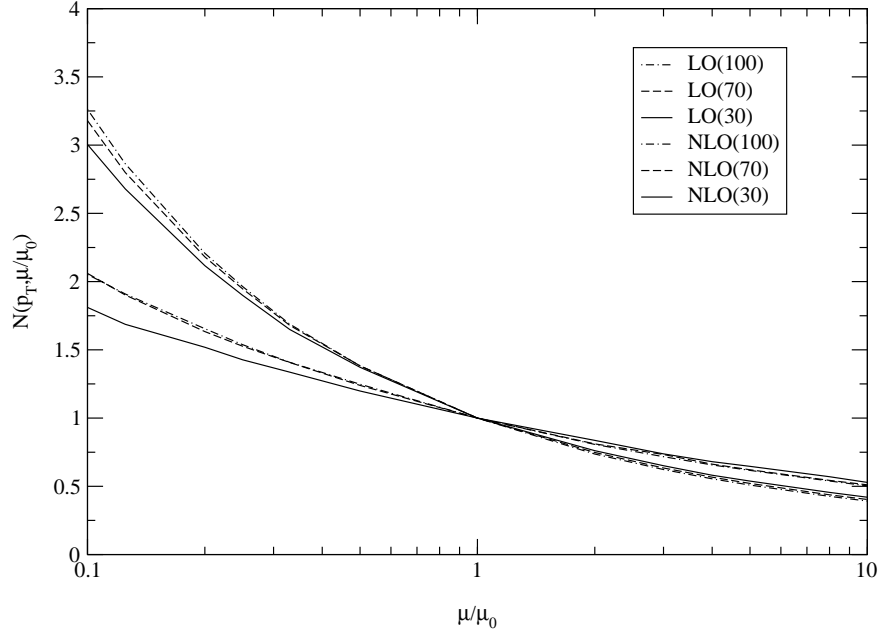


Figure 3: The quantity $N(p_T; =_0)$ (see Eq. (3.14)), plotted in the range $0.1 < =_0 < 10$ at fixed values of p_T with $m_H = 120 \text{ GeV}/c^2$ and $=_0^2 = m_H^2 + p_T^2$ using the MRST98 parton density sets. The results are shown for $p_T = 30 \text{ GeV}/c$ (solid line), $p_T = 70 \text{ GeV}/c$ (dashed line), $p_T = 100 \text{ GeV}/c$ (dot-dashed line). The upper three curves on the left hand side are the LO results whereas the lower three curves refer to NLO.

indicated by the K -factor defined by

$$K = \frac{d^{\text{NLO}}}{d^{\text{LO}}} : \quad (3.15)$$

Depending on the parton density set the K -factors are pretty large and vary from 1.4 at $p_T = 30 \text{ GeV}/c$ to 1.7 at $p_T = 150 \text{ GeV}/c$ for both H and A production. Another uncertainty is the dependence of the p_T distribution on the specific choice of parton densities, which can be expressed by the factors like

$$R^{\text{CTEQ}} = \frac{d^{\text{CTEQ}}}{d^{\text{MRST}}} ; \quad R^{\text{GRV}} = \frac{d^{\text{GRV}}}{d^{\text{MRST}}} ; \quad (3.16)$$

and are generally above unity. Again these factors are essentially identical for H and A production. For specific values consult [18], [19], [21] and [22].

The reason why the parton density sets yield different results for the p_T -distributions can be mainly attributed to the small- x -behaviour of the gluon density because gluon-gluon fusion is the dominant production mechanism. Future HERA data will have to provide us with unique gluon densities before we can make more accurate predictions for the Higgs differential distributions.

4 Numerical results at large x .

Near threshold the longitudinal momentum fractions x_i approach unity. In this region the soft-plus-virtual (S+V) gluons and collinear $q\bar{q}$ pairs dominate the NLO corrections to the partonic cross sections. The S+V gluon parts of these cross sections are obtained by omitting the hard

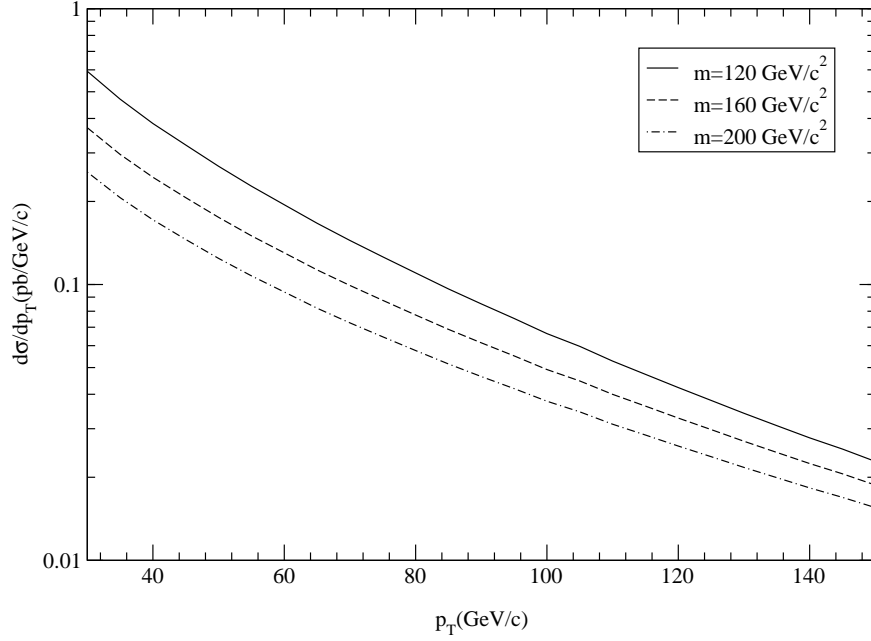


Figure 4: The m dependence of d^{NLO}/dp_T (see Eq. (3.13)) using the set MRST 99 (cor01.dat) with $s^2 = m_H^2 + p_T^2$ for Higgs masses $m_H = 120 \text{ GeV}/c^2$ (solid line), $m_H = 160 \text{ GeV}/c^2$ (dashed line) and $m_H = 200 \text{ GeV}/c^2$ (dot-dashed line).

contributions which are regular at $s_4 = (p_3 + p_4)^2 = 0$ and adding the pieces from the virtual contributions. These two contributions constitute the S+V gluon approximation. To study its validity we show in Fig. 5 the ratio

$$R^{\text{S+V}} = \frac{d^{\text{S+V}}}{d^{\text{EXACT}}}; \quad (4.17)$$

for the NLO contributions to the p_T distribution (here $p_{T,\text{min}} = 30 \text{ GeV}/c$). One expects that the approximation becomes better at larger transverse momenta where p_T approaches the boundary of phase space at $x = 1$. However in Fig. 5 the highest value of p_T , given by $p_T = 150 \text{ GeV}/c$, is still very small with respect to $p_{T,\text{max}} = \sqrt{s} = 7 \cdot 10^3 \text{ GeV}/c$. Therefore it is rather fortuitous that the approximation works so well for $p_T > 100 \text{ GeV}/c$ where one obtains $R^{\text{S+V}} < 1.2$.

The S+V gluon approximation overestimates the exact NLO result but the difference decreases when the p_T increases. In particular for $p_T > 200 \text{ GeV}/c$ the S+V approximation is good enough so that resummation techniques could be used to give a better estimate of the Higgs boson p_T distribution corrected up to all orders in perturbation theory. Note that the boundary of phase space is also approached when m_B increases at fixed p_T , but, according to the results in Fig. 5, the S+V approximation does not improve. In [21] it was noted that increasing m_B makes the terms in $\ln(m_B/p_T)$ larger at fixed p_T . So the range in p_T where the small p_T -logarithms dominate increases with increasing m_B . This leads us to the next topic.

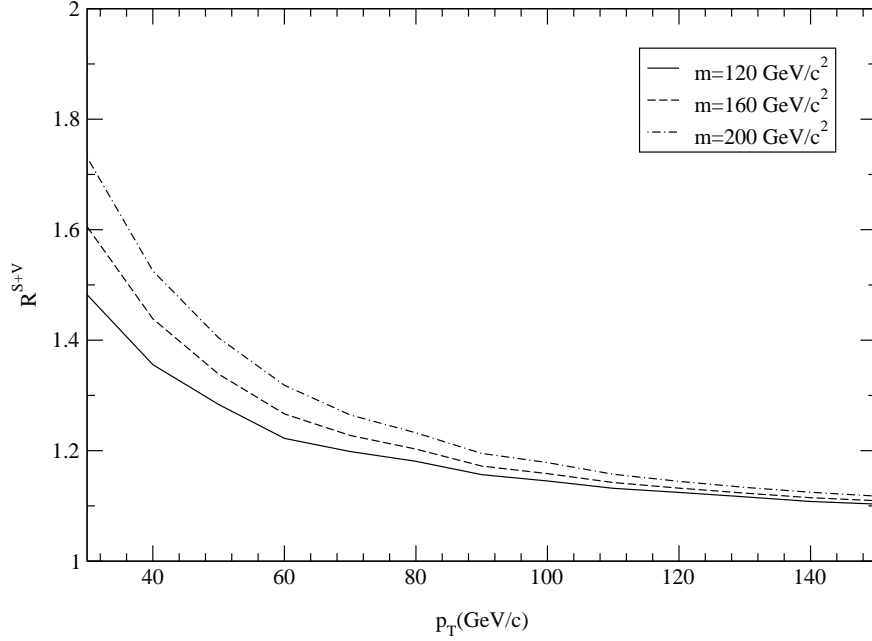


Figure 5: The ratio R^{S+V} in Eq. (4.17) for the p_T distributions using the set MRST99 (cor01.dat) with $s^2 = m_H^2 + p_{T,\min}^2$ and various Higgs masses given by $m_H = 120 \text{ GeV}/c^2$ (solid line), $m_H = 160 \text{ GeV}/c^2$ (dashed line) and $m_H = 200 \text{ GeV}/c^2$ (dot-dashed line).

5 Numerical results at small p_T

We noted previously that there are terms in $m_B = p_T \ln^i(m_B = p_T)$ which are dominant in the small p_T region. In this region the double differential cross section can be expanded as follows

$$\frac{d}{dp_T^2 dy} = \frac{\sigma_0 m_B^2}{s p_T^2} \sum_{m=1}^{\infty} \sum_{n=0}^{\infty} \frac{x^{2m-1}}{2} C_{mn} \ln \frac{m_B^2}{p_T^2}^n + \dots; \quad (5.18)$$

where the next order terms start with $m = 3$ (order s^3), and σ_0 denotes one of the partonic cross sections for the LO processes in Eq.(2.1), which are order s^2 . In [21] the C_{mn} were determined from their explicit NLO results in terms of certain factors $A^{(1)}, A^{(2)}, B^{(1)}, B^{(2)}, C_{gg}^{(1)}, C_{gq}^{(1)}$ which multiply convolutions of splitting functions with parton densities. These factors had been previously determined in [32], [33] from other reactions, so it was gratifying to see the consistency between the different results. In Fig. 6 we show a comparison of the inclusive result in Eq. (3.9) at both LO and NLO versus the corresponding result from the small p_T -limit formula in Eq. (5.18). The latter works very well for p_T smaller than 10 GeV/c and agrees with the exact calculation for p_T smaller than 5 GeV/c. The authors then propose another large x approximation involving both the $S+V$ and small p_T terms. We refer to their paper for details.

Note that the resummation of the logarithms in Eq. (5.18) can be carried out following the procedure in [34]. This leads to a change in the shape of the p_T -spectrum at small p_T . Results can be found in [35], [36], [37].

In conclusion we note that the NLO corrections to the B differential distributions are now completely known and resummation methods have been used to study the region near $p_T = 0$.

Acknowledgement: We thank C. G. Bosser and C. Schmidt for giving us the inputs for Fig.6. We also thank B. Field, M. Tejeda-Yeomans, S. Dawson, R. Kaurman, D. de Florian, M. Grazzini and Z. Kunszt for discussions and comments.

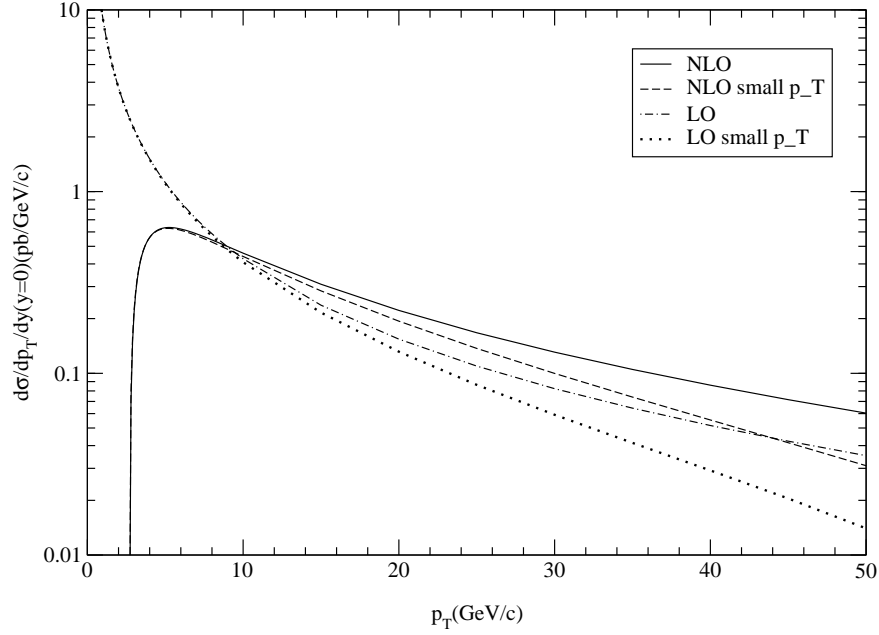


Figure 6: The Higgs p_T spectrum compared to the small- p_T limit formula (see Eq. (5.18)) at both LO and NLO with CTEQ 5L and CTEQ 5M1 parton densities respectively. All curves are calculated for $y = 0$ in the $m_t = 174$ GeV effective theory.

References

- [1] S.L. Glashow, Nucl. Phys. 22,579 (1961); A. Salam, Elementary Particle Theory, Nobel Symposium, No.8, ed. N. Svartholm (Stockholm: Almqvist and Wiksell Forlag A.B. 1968). p.367; S.W einberg, Phys. Rev. Lett. 19,1264 (1967).
- [2] P.W. Higgs, Phys.Lett. 12,132 (1964); Phys. Rev. Letts. 13,508 (1964); Phys. Rev. 145,1156 (1966); F. Englert and R. Brout, Phys. Rev. Lett. 13,321 (1964); G.S. Guralnik, C.R. Hagen and T.W. Kibble, Phys. Rev. Letts. 13,585 (1964).
- [3] R. Barate et al. (ALEPH Collaboration), Phys. Lett. B 495,1 (2000), hep-ex/001145; M. Acciarri et al. (L3 Collaboration), Phys. Lett. B 508,225 (2001), hep-ex/0012019; P. Abreu et al. (DELPHI Collaboration), Phys. Lett. B 499,23 (2001), hep-ex/0102036; G. Abbiendi et al. (OPAL Collaboration), Phys. Lett. B 499,38 (2001), hep-ex/0101014.
- [4] J.F. Gunion, H.E. Haber, G.L. Kane and S. Dawson, The Higgs Hunter's Guide, (Addison-Wesley, Reading, M.A., 1990), Erratum ibid. hep-ph/9302272.
- [5] LEP Collaborations, CERN-EP/2001-055 (2001), hep-ex/0107029;
LEP Higgs Working Group, hep-ex/0107030;
P. Igo-Kemenes, in K. Hagiwara, et al. (Eds), Review of Particle Physics, Phys. Rev. D 66,010001 (2002).
- [6] D. Rainwater, M. Spira and D. Zeppenfeld, hep-ph/0203187; M. Spira, hep-ph/0211145, S. Dawson, hep-ph/0111226.

- [7] F. Wilczek, Phys. Rev. Lett. 39,1304 (1977); H. Georgi, S. Glashow, M. Machacek, D. Nanopoulos, Phys. Rev. Lett. 40,692 (1978); J. Ellis, M. Gaillard, D. Nanopoulos, C. Sachrajda, Phys. Lett. B 83,339 (1979); T. Rizzo, Phys. Rev. D 22,178 (1980).
- [8] R. K. Ellis, I. Hinchli, M. Soldate, J. J. van der Bij, Nucl. Phys. B 297,221 (1988); U. Baur, E. W. Glover, Nucl. Phys. B 339,38 (1990); R. P. Kauaman, Phys. Rev. D 44,1415 (1992); *ibid* Phys. Rev. D 45, 1512 (1992).
- [9] C. Kao, Phys. Lett. B 328, 420 (1994), hep-ph/9310206.
- [10] S. Dawson, Nucl. Phys. B 359,283 (1991); R. P. Kauaman, W. Schaer, Phys. Rev. D 49, 551 (1994); S. Dawson, R. P. Kauaman, Phys. Rev. D 49, 2298 (1994).
- [11] A. Djouadi, M. Spira and P. M. Zerwas, Phys. Lett. B 264,440 (1991); D. Graudenz, M. Spira, P. M. Zerwas, Phys. Rev. Lett. 70,1372 (1993); M. Spira, A. Djouadi, D. Graudenz, P. Zerwas, Phys. Lett. B 318,347 (1993).
- [12] M. Spira, A. Djouadi, D. Graudenz, P. Zerwas, Nucl. Phys. B 453, 17 (1995), hep-ph/9504378.
- [13] V. Del Duca, W. Kilgore, C. Oleari, C. Schmidt and D. Zeppenfeld, Phys. Rev. Lett. 87,122001 (2001), hep-ph/0105129; *ibid* Nucl. Phys. B 616,367 (2001), hep-ph/0108030.
- [14] M. Kramer, E. Laenen and M. Spira, Nucl. Phys. B 511,523 (1998), hep-ph/9611272.
- [15] S. Dawson, R. P. Kauaman, Phys. Rev. Lett. 68,2273 (1992); R. P. Kauaman, S. V. Desai, D. Risal, Phys. Rev. D 55,4005 (1997), Erratum *ibid*. D 58,119901 (1998), hep-ph/9610541.
- [16] R. P. Kauaman, S. V. Desai, Phys. Rev. D 59,05704 (1999), hep-ph/9808286.
- [17] C. R. Schmidt, Phys. Lett. B 413,391 (1997), hep-ph/9707448.
- [18] D. de Florian, M. Grazzini, Z. Kunszt, Phys. Rev. Lett. 82, 5209 (1999), hep-ph/9902483.
- [19] V. Ravindran, J. Smith, W. L. van Neerven, Nucl. Phys. B 634,247 (2002), hep-ph/0201114.
- [20] C. J. Glosser, hep-ph/0201054.
- [21] C. J. Glosser and C. R. Schmidt, JHEP 0212,016 (2002), hep-ph/0209248.
- [22] B. Field, J. Smith, M. E. Tejeda-Yeomans, W. L. van Neerven, Phys. Lett. B 551,137 (2003), hep-ph/0210369.
- [23] B. Field, Phys. Rev. D 66,114007 (2003), hep-ph/0208262.
- [24] K. G. Chetyrkin, B. A. Kniehl, M. Steinhauser, Phys. Rev. Lett. 79, 353 (1997), hep-ph/9705240.
- [25] K. G. Chetyrkin, B. A. Kniehl, M. Steinhauser, W. A. Bardeen, Nucl. Phys. B 535,3 (1998), hep-ph/9807241.
- [26] S. L. Adler, W. Bardeen, Phys. Rev. 182,1517 (1969).

- [27] A.D. Martin, R.G. Roberts, W.J. Stirling and R.S. Thorne, Eur. Phys. J. C 4, 463 (1998), hep-ph/9803445.
- [28] A.D. Martin, R.G. Roberts, W.J. Stirling and R.S. Thorne, Eur. Phys. J. C 14, 133 (2000), hep-ph/997231.
- [29] M. Glück, E. Reya, A. Vogt, Eur. Phys. J. C 5, 461 (1998), hep-ph/9806404.
- [30] H. Lai et al, Phys. Rev. D 55, 1280 (1997), hep-ph/9606399.
- [31] H.L. Lai et al [CTEQ Collaboration] Eur. Phys. J. C 12, 375 (2000), hep-ph/9903282.
- [32] P.B. Arnold and R.P. Kauaman, Nucl. Phys. B 349, 381 (1991).
- [33] S. Catani, D. de Florian, M. Grazzini, Nucl. Phys. B 596, 299 (2001), hep-ph/0008184.
- [34] J.C. Collins, D.E. Soper, Nucl. Phys. B 193, 381 (1981) [Erratum ~~ibid~~ B 213, 545 (1983)]; J.C. Collins, D.E. Soper, Nucl. Phys. B 197, 446 (1982); J.C. Collins, D.E. Soper, G. Sterman, Nucl. Phys. B 250, 199 (1985).
- [35] I. Hinchli e, S.F. Novaes, Phys. Rev. D 38, 3475 (1988); R.P. Kauaman, Phys. Rev. D 44, 1415 (1991); R.P. Kauaman, Phys. Rev. D 45, 1512 (1992); S. Catani, E. De Renzi and L. Trentadue, Phys. Lett. B 211, 335 (1988); C.-P. Yuan, Phys. Lett. B 283, 395 (1992) 395; C. Balazs and C.-P. Yuan, Phys. Rev. D 59, 111407 (1999), Erratum ~~ibid~~. D 63 (2001) 059902, ~~ibid~~. Phys. Lett. B 478, 192 (2000), hep-ph/0001103; C. Balazs, J. Huston and I. Puljak, Phys. Rev. D 63, 014021, 014021 (2001);
- [36] D. de Florian and M. Grazzini, Phys. Rev. Lett. 85, 4678 (2000), hep-ph/0008152; D. de Florian and M. Grazzini, Nucl. Phys. 616, 247 (2001); hep-ph/0108273. G. Bozzi, S. Catani, D. de Florian and M. Grazzini, Phys. Lett. B 564, 65 (2003).
- [37] E.L. Berger and J. w. Qiu, Phys. Rev. D 67 034026 (2003) E.L. Berger and J. w. Qiu, hep-ph/0304267.